RESEARCH ARTICLE

Key Points:
- Explain how seismic interferometry extracts waveforms at caustics
- At caustics the stationary phase zones are very large
- This explains observations of waveforms extracted at caustics (e.g., antipodes)

Correspondence to:
R. Snieder,
rsnieder@mines.edu

Seismic interferometry and stationary phase at caustics

Roel Snieder[1,2] and Christoph Sens-Schönfelder[1]

[1]Deutsches GeoForschungsZentrum, Potsdam, Germany, [2]Center for Wave Phenomena, Colorado School of Mines, Golden, Colorado, USA

Abstract Waves that propagate between two receivers can be extracted by cross correlating noise recorded at these receivers if the noise is generated by sources on a closed surface surrounding the receivers. This concept is called seismic interferometry. Of all these noise sources, those for whom the travel time difference for propagation to the two receivers is in the stationary phase zone, give the dominant contribution. In this paper we analyze the stationary phase properties when one receiver is at a caustic for waves leaving the other receiver. A simple model for a waveguide and a general treatment of caustics show that, at a caustic, the curvature of the travel time difference at the stationary phase zone vanishes. As a result the stationary phase region is considerably wider at a caustic than at other points, and it is more likely that noise sources are present in the stationary phase region. This explains why it is easier to extract waves from seismic interferometry when the receivers are at caustics such as antipodal receivers on the Earth.

1. Introduction

Seismic interferometry is a technique where one retrieves waves that propagate between two receivers by cross correlating random wave fields recorded at these two receivers. As a result, one of these receivers acts as a source, even though no physical source is present; for this reason one speaks of a *virtual source* [*Bakulin and Calvert*, 2006]. Under optimal conditions the retrieved waves are the impulse response or Green's function. In order to extract the Green's function, sources must, strictly speaking, radiate energy homogeneously along a closed surface that surrounds the receivers. The principle of seismic interferometry is discussed in a number of review papers [*Curtis et al.*, 2006; *Larose et al.*, 2006; *Snieder and Larose*, 2013].

Mathematically, the principle of seismic interferometry for acoustic waves is given by equation (32) of *Wapenaar and Fokkema* [2006]:

$$G(\mathbf{r}_A, \mathbf{r}_B, \omega) - G^*(\mathbf{r}_A, \mathbf{r}_B, \omega) = -\frac{2i\omega}{\rho c} \oint G(\mathbf{r}_B, \mathbf{r}, \omega) G^*(\mathbf{r}_A, \mathbf{r}, \omega) \mathrm{d}^2 r \,, \tag{1}$$

where G is the Green's function, the asterisk denotes complex conjugation, ρ is the mass density, c the velocity, and ω the angular frequency. Because of the complex conjugation, the phase of $G(\mathbf{r}_B, \mathbf{r}, \omega)$ and $G^*(\mathbf{r}_A, \mathbf{r}, \omega)$ in the integrand is subtracted, which corresponds, in the time domain, to a subtraction of arrival times.

According to equation (1), one needs sources all along a closed surface that surrounds the receivers. These sources can be true noise sources, reflection points, or scatterers. The latter two source types act as secondary sources. In practice, one does not need sources everywhere to retrieve the arrival of waves that propagate between the receivers. The dominant contribution to the interferometric integral (1) comes from stationary phase regions [*Snieder*, 2004; *Snieder et al.*, 2006, 2008]. These are areas where the phase of the integral (1) does not change to first order with the location of the source on the enclosing surface. (The stationary phase regions are also called coherency zones [*Larose*, 2006] or end-fire lobes [*Roux et al.*, 2004]).

In practice, it has proven to be relatively easy to extract surface waves from seismic interferometry [*Campillo and Paul*, 2003], and this technique has revolutionized crustal surface wave tomography [*Campillo et al.*, 2011; *Ritzwoller et al.*, 2011]. It has proven to be more difficult to extract body waves from the cross correlation of noise [*Draganov et al.*, 2009; *Nakata et al.*, 2011] than it is for surface waves. Assuming that noise sources are only present at the Earth's surface, stationary phase zones are much larger for surface waves than for body waves [*Forghani and Snieder*, 2010]. As a result, it is more likely for sources to be located in the stationary phase regions of surface waves than it is for body waves. In addition, the ability to extract body waves and
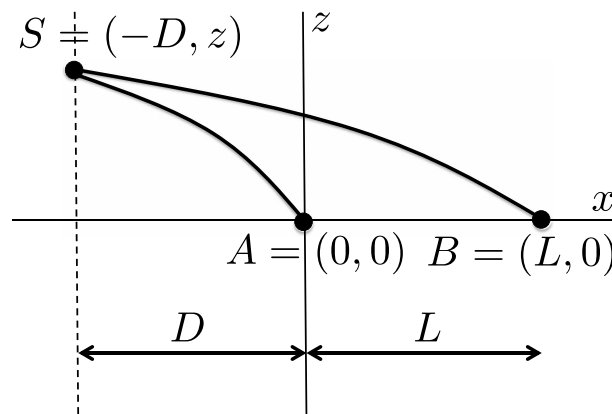
Figure 1. Definition of geometric variables for receivers on the x axis and sources on the dashed line $x = -D$.

surface waves by cross correlation of ambient noise also depends on the degree to which these wave types are present in the noise field. The seismic noise is strongest in the microseismic band where it is dominated by surface waves [*Schulte-Pelkum et al.*, 2004; *Stehly et al.*, 2006], although body waves are also present in seismic noise [*Gerstoft et al.*, 2008; *Zhang et al.*, 2009]. A comprehensive theory of the generation of seismic noise is given by *Traer and Gerstoft* [2014].

Reflected body waves have been retrieved from teleseismic waves using deconvolution [*Bostock and Rondenay*, 1999; *Bostock et al.*, 2002; *Kumar and Bostock*, 2006] and cross correlation [*Ruigrok et al.*, 2011]. Seismic interferometry has also been used to extract and enhance refracted waves from active shot experiments [*Mikesell and van Wijk*, 2011] and core-diffracted waves from earthquakes [*Bharadwaj et al.*, 2014]. Moho-reflected waves, both *PmP* and *SmS*, have been extracted from the cross correlation from ambient noise [*Zhan et al.*, 2010; *Poli et al.*, 2012a]. Recently, a number of studies have shown that body waves that propagate deep in the Earth can be extracted by cross correlation of either ambient noise or earthquake coda [*Poli et al.*, 2012b; *Nishida*, 2013; *Boué et al.*, 2013; *Lin and Tsai*, 2013; *Lin et al.*, 2013]. Some of these studies use averaging provided by array measurements to reconstruct the body wave arrivals, but *Lin and Tsai* [2013] retrieved body waves for individual station pairs located at antipodes. The large amplitudes of retrieved teleseismic waves at a distance of about 150° near the triplication of core phases [*Nishida*, 2013; *Boué et al.*, 2013] suggest that the retrieval of body waves in seismic interferometry is enhanced when receivers are located near caustics.

The purpose of this paper is to show how the vicinity of caustics near receivers assist in the extraction of waves from seismic interferometry. *Boué et al.* [2014] postulate that reverberations in the Earth facilitate the extraction of body waves because of the large stationary phase regions for such wave paths. In this paper we explore and elucidate this postulate for the related problem of the extraction of waves near caustics by seismic interferometry. We present in section 2 a model of a waveguide as a simple prototype of a velocity structure that produces caustics. In section 3 we show numerically how the rays and travel times behave in this model and show how the stationary phase region changes at a caustic. We extend this to general caustics in section 4. We show in section 5 how the large stationary phase zone at caustics affects the integration over sources and discuss the implications for the interferometric retrieval of waves near caustics in section 6. Appendix A contains mathematical details of ray theory in the waveguide model.

2. Caustics in a Waveguide

We present the behavior of seismic interferometry at caustics with a simple 2-D example of waves that propagate in a waveguide. In this model the wave velocity c depends on depth only and is given by

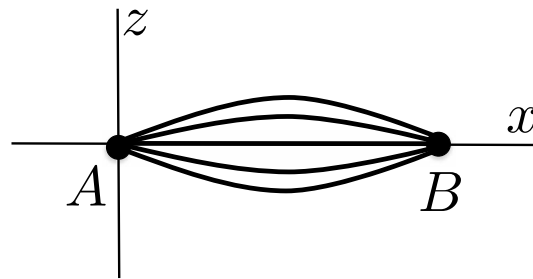$$\frac{1}{c(z)} = \frac{1}{c_0}\left(1 - \frac{1}{2}q^2 z^2\right),\tag{2}$$

where c_0 and q are positive constants. We consider the geometry shown in Figure 1 where rays propagate from a source at location $S = (-D, z)$ to receivers at locations $A = (0, 0)$ and $B = (L, 0)$ that are located on the axis of the waveguide. As shown in Appendix A, these rays are approximately given by

$$z(x) = z\frac{\sin q(-x)}{\sin qD}\quad\text{(ray SA)},\tag{3}$$

$$z(x) = z\frac{\sin q(L - x)}{\sin q(L + D)}\quad\text{(ray SB)},\tag{4}$$

Figure 2. Rays propagating from a source at A to a caustic at B.

As expected, the rays oscillate around the axis of the wave guide. When the rays cross the wave guide axis, they go through a caustic. This happens periodically over each propagation distance π/q, and we show in Appendix A that a ray propagating over a distance X along the x axis is at a caustic when

$$\sin qX = 0 \quad \text{(caustic)} . \tag{5}$$

This means, for example, in equation (3), that at a caustic $\sin qD = 0$. In the vicinity of the caustic $\sin qD \to 0$; hence, to analyze the ray behavior at a caustic, we set $\sin qD = \varepsilon$. For an initial ray position $z = \varepsilon a$, equation (3) states that in that case $z(x) = -a \sin qx$. This means that at the caustic ($\varepsilon = 0$), rays with nonzero ray deflection connect the source and receives on the x axis. This corresponds to the fact that at a caustic, nearby rays connect the same points, see the sketch in Figure 2. We make this statement more precise in expression (15).

We focus in this work on stationary phase principles in seismic interferometry. For the stationary phase analysis we study the variation of the travel time as a function of the source position z. We denote the nth-order variation of the travel time with z as $t^{(n)}$:

$$t = t^{(0)} + t^{(2)} + O(z^3) . \tag{6}$$

The zeroth-order variation $t^{(0)}$ is the travel time for the ray starting at $z = 0$ that propagates along the x axis. The first-order variation $t^{(1)}$ vanishes, which is consistent with Fermat's theorem [*Aldridge*, 1994; *Snieder and van Wijk*, 2015]. The second-order variation $t^{(2)}$ is, by definition, proportional to z^2. This variation gives the curvature of the travel time with the z coordinate of the starting point of the ray. If follows from expressions (A7) and (A8) in Appendix A that for the rays SA and SB, the zeroth- and second-order travel time variations are given by

$$t_{SA}^{(0)} = \frac{D}{c_0} \quad \text{and} \quad t_{SA}^{(2)} = \frac{qz^2}{2c_0 \tan qD} , \tag{7}$$

$$t_{SB}^{(0)} = \frac{L+D}{c_0} \quad \text{and} \quad t_{SB}^{(2)} = \frac{qz^2}{2c_0 \tan q(L+D)} , \tag{8}$$

According to expression (1), one cross correlates in seismic interferometry waves recorded at receivers A and B to retrieve the waves that propagate between these receivers. Cross correlation corresponds, in the time domain, to a subtraction of travel times. For this reason we can subtract the travel times from the source S to the receivers A and receiver B to estimate the contribution of a source at location S to the interferometric integral (1). Following expression (7), this difference is to zeroth order in z given by

$$t_{SB}^{(0)} - t_{SA}^{(0)} = \frac{L}{c_0} . \tag{9}$$

This is just the travel time of a wave that propagates along the x axis from A to B. According to expressions (7) and (8), the second-order contribution of the travel time is given by

$$t_{SB}^{(2)} - t_{SA}^{(2)} = \frac{qz^2}{2c_0} \left(\frac{1}{\tan q(L+D)} - \frac{1}{\tan qD} \right) . \tag{10}$$

Using trigonometric identities, this can be written as

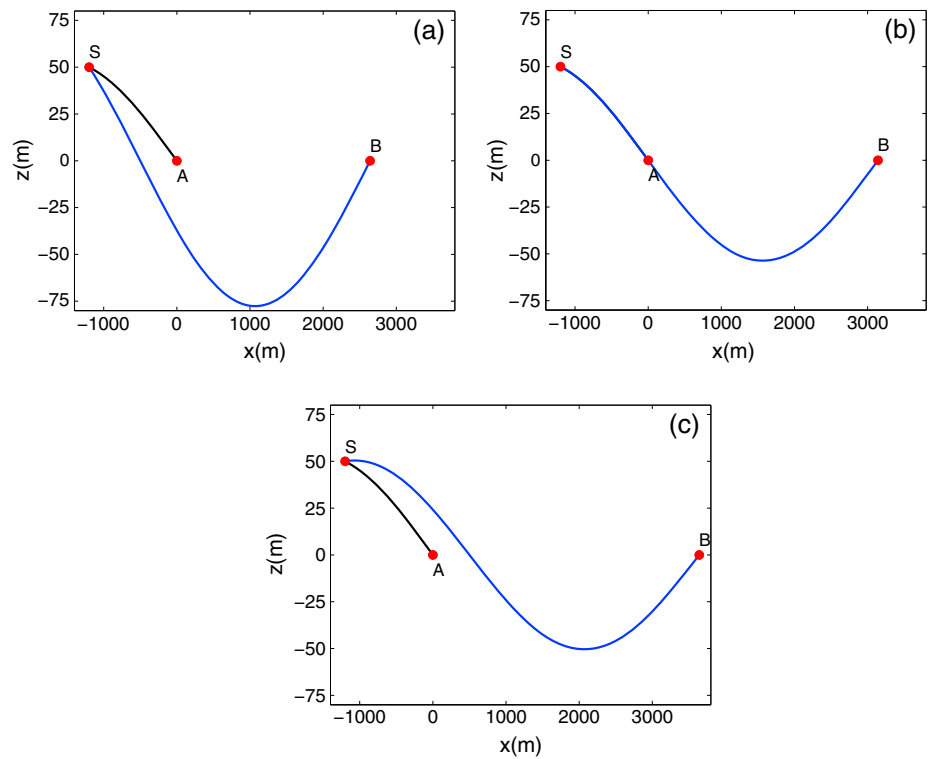$$t_{SB}^{(2)} - t_{SA}^{(2)} = \frac{qz^2}{2c_0} \frac{\sin qL}{\sin q(L+D) \sin qD} . \tag{11}$$

Figure 3. Rays ending at the points A and B when: AB is 500 m (a) before the caustic, (b) at the caustic, and (c) beyond the caustic. Note the exaggeration of the scale along the vertical axis.

Following equation (5), $\sin qL = 0$ when B is at a caustic for waves launched in A because these points are separated by a distance L. Under these conditions expression (11) states that

$$t_{SB}^{(2)} - t_{SA}^{(2)} = 0 \quad \text{(caustic)} . \tag{12}$$

This means that the curvature of the travel time as a function of z for waves traveling from S to A and from S to B, respectively, is equal. According to the classic stationary phase analysis applied to interferometry, it is this difference $t_{SB}^{(2)} - t_{SA}^{(2)}$ that determines the amplitude and phase of the waves inferred from seismic interferometry [*Snieder*, 2004]. This quadratic term vanishes at a caustic, which means that the asymptotic evaluation of the integration (1) over sources now depends on the third- or higher-order dependence of the travel time on source position z [*Bender and Orszag*, 1978]. Because the problem in Figure 1 is symmetric in z, the third-order term in the travel time expansion (6) vanishes, which means that when B is at a caustic for rays leaving A, the travel time varies to leading order as the fourth power of the source position: $t = t^{(0)} + t^{(4)}$. Rather than asymptotically evaluating the resulting integral, we illustrate this situation with a numerical example.

3. Numerical Example

In the numerical example we use expression (2) with $c_0 = 1500$ m/s and $q = 1/1000$ m. According to expression (5) the first caustic occurs when $L = \pi/q = 3141$ m. Sources are located 1200 m to the left of the first receiver: $D = 1200$ m. Figure 3a shows rays leaving a sample source at $z = 50$ m that propagate to the receivers when receiver B is located 500 m before the first caustic: $L = 2641$ m.

We compute the travel time for each ray by numerically integrating expression (A6) along the ray. The travel time t_{SA} for the rays SA as a function of source position z is shown by the black line in Figure 4, while the travel time t_{SB} for rays SB is indicated by the blue line. The difference $t_{SB} - t_{SA}$ of the travel times is indicated by the red line. At this scale the travel time curves are lines that appear to be straight. This is not very informative for the stationary phase analysis of the interferometric integral (1) because the stationary phase analysis depends on the *variation* of the travel time difference with the source position z. To show this variation, we subtract from
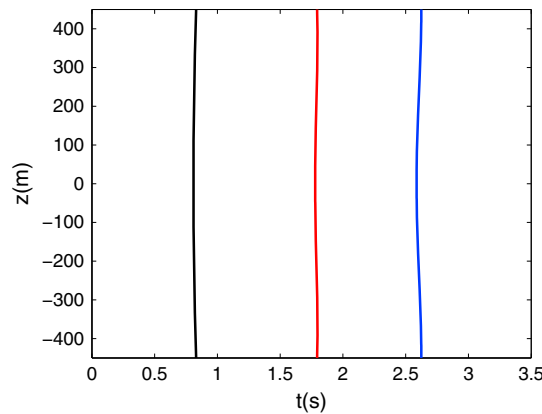
Figure 4. Travel times for the rays in the left side of Figure 3 that end at point A (black line) and point B (blue line) as a function of the z coordinate of the source when AB is 500 m before the caustic. Red line shows the difference in these travel times.

each of these curves the travel time for a source at $z = 0$ resulting in the reduced travel time:

$$t_{\text{reduced}}(z) \equiv t(z) - t(z = 0) . \qquad (13)$$

The reduced travel times for the rays in Figure 3a are shown in Figure 5a. In this case the rays propagating to both receivers have a positive curvature with z (black and blue curves) indicating that travel times grow with increasing distance from the axis of the wave guide. The travel time difference has a positive curvature as well (red curve). Such a positive curvature also occurs in the case of velocity structures that do not form caustics, and a stationary phase evaluation of the interferometric integral (1) is similar to the evaluation shown by *Snieder* [2004]. The dominant contribution to this integral comes from the stationary phase zone for the red curve. For waves with a period T the stationary phase region is defined as the region where the reduced travel time difference (red curve) for rays SA and SB is less than about a quarter wavelength:

$$|t_{\text{reduced},SB}(z) - t_{\text{reduced},SA}(z)| < T/4 . \qquad (14)$$

For symmetry reasons the stationary phase region always includes the sources at $z = 0$ and its width is determined by the curvature of $t_{\text{reduced},SB}(z) - t_{\text{reduced},SA}(z)$.
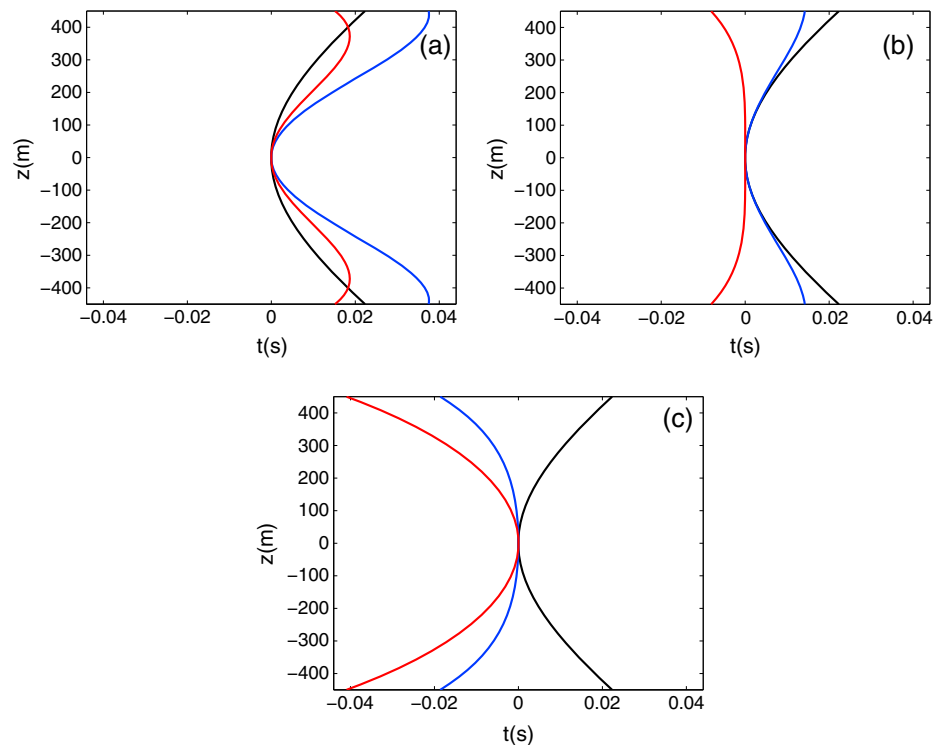

Figure 5. Travel times relative to the travel time at $z = 0$ for the rays in Figure 3 that end at point A (black line) and point B (blue line) as a function of the z coordinate of the source position. Red line shows the difference in these travel times. (a) Rays with AB 500 m before the caustic, (b) when AB is at the caustic, and (c) for AB 500 m beyond the caustic.

The rays in Figure 3b illustrate the case when $L = 3141$ m. In this case receiver B is at a caustic for rays leaving receiver A, but neither receiver A nor receiver B are at a caustic for rays leaving the source S. At the caustic the ray-geometric amplitude is infinite, but since neither receiver is at a caustic of rays leaving the source S, the ray-geometric wave fields that are cross correlated both have finite amplitude. The wave that propagates from A to B is, however, at a caustic, and therefore has a large amplitude. This amplitude is not infinite because the wavefield at a caustic is finite, only the ray-geometric approximation diverges.

How does the interferometric integral (1) reproduce the large amplitude at caustics? As shown in Figure 3b, the ray propagating from the source to B (blue line) is for the leftmost part SA virtually identical to the ray that propagates from the source to A. From A onward, the ray then propagates from A to B. For this source position, the travel time difference of rays that propagate from S to B and from S to A is equal to the travel time of waves that propagate from A to B. So the shown source in Figure 3b is in the stationary phase zone of the receivers A and B even though it is not located on the x axis. Effectively, the stationary phase zone is in this case much broader than it is when B is not in a caustic for waves launched at A.

Away from caustics, as shown in Figures 3a and 5a, the ray that propagates from S to A does not continue as the ray that propagates from A to B. The only exception is when the source is located on the x axis at $z = 0$, in that case rays propagate along the x axis from S to A and B which limits the stationary phase zone to a narrow area around $z = 0$. But when B is at a caustic for waves leaving A, as shown in Figure 3b, sources for $z \neq 0$ also launch waves that almost exactly go through receiver A before traveling to receiver B. This effectively gives a much larger stationary phase region, which produces the large amplitude of the wave recorded at the caustic. It reflects the fact that point B is at a caustic when to leading order in the take-off direction, the endpoint of rays that leave A does not change (Figure 2).

A different way to look at this situation is to consider the reduced travel time shown in Figure 5b. In this case, the travel time curves for receivers A and B (blue and black lines) again have a positive curvature. Near the stationary phase point $z = 0$, the curvature of the black and blue lines is virtually identical. As a result, the difference of the travel times (red curve) has a vanishing curvature at the stationary phase zone: $\partial^2(t_{\text{reduced,SB}} - t_{\text{reduced,SA}})/\partial z^2 = 0$. This cancelation of the curvature of the second-order travel time variation with z at the receivers A and B is predicted by equation (12). A second-order stationary-phase analysis, such as that used by *Snieder* [2004] predicts an infinite amplitude. Such a second-order stationary-phase analysis corresponds to extracting the ray-geometric amplitude, which is indeed infinite. But a proper stationary phase analysis takes the first leading order variation into account [*Bender and Orszag*, 1978], which is in this case of fourth order. The red curve in Figure 5b indeed shows a fourth-order variation with z. Because of the slow variation of the reduced travel time with z, the stationary phase condition (14) now corresponds to a much wider stationary phase region than in Figure 3a. This wider stationary phase region produces the large, but finite, amplitude that is characteristic of waves as a caustic.

Figures 3c and 5c show the rays and reduced travel times for a receiver separation $L = 3614$ m. In this case, receiver B is 500 m beyond the caustic for rays leaving A. Consequently, the ray propagating to receiver B (Figure 3c) now does not propagate through receiver A. The curvature of the travel times, as shown by the black and blue lines in Figure 5c are different. The curvatures of these travel time curves now have an opposite sign, and the difference of the travel times (red curve in Figure 5c) has a negative curvature too. According to expression (24.38) of *Snieder and van Wijk* [2015], this change in curvature corresponds, after integration over z, to a phase shift $\exp(i\pi/2)$. In the time domain this phase shift corresponds to a Hilbert transform [*Aki and Richards*, 2002]. The Hilbert transform occurs when a wave goes through a caustic where the Maslow index increases by 1 [*Chapman*, 2004]. The red travel time curves in Figure 5 show that the travel time difference has a positive curvature before the caustic (red line in Figure 5a) and a negative curvature beyond the caustic (red line in Figure 5c). Since the travel time difference changes curvature continuously, there must be an intermediary point where the curvature vanishes. As shown by the red line in Figure 3b, the curvature changes sign exactly at the caustic.

4. General Caustics

The previous example was for the special case of the wave guide (2) for the geometry of Figure 1. The principles carry over to a more general caustic as shown in Figure 6. These cases also include structures with asymmetric velocity profiles such as a SOFAR channel. (This is the Sound Fixing and Ranging acoustic waveguide in the ocean that allows sound to propagate over large distances [*Dietrich et al.*, 1980]). Suppose a ray propagates
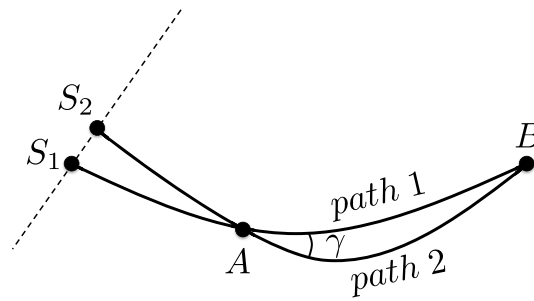
Figure 6. The perturbation of a ray path near a caustic.

along path 1 from S_1 to A and continues to B. One can perturb the take-off angle γ and launch a wave along path 2. When B is at a caustic, the ray along another path 2 still goes through B, this is the situation depicted in Figure 2. In fact, at a caustic, the travel time of the waves does, to second order, not change with the take-off angle [*Berry and Upstill*, 1980]:

$$\frac{\partial^2 t_{AB}}{\partial \gamma^2} = 0 \quad \text{(caustic)} \tag{15}$$

In an interferometric experiment, an infinitesimal change in the take-off angle that changes path 1 into path 2, corresponds to a change in the source position from S_1 to S_2 (Figure 6). For both source positions, the rays travel through receiver A to receiver B; hence, $t_{SB} - t_{SA} = t_{AB}$, and equation (15) thus states that at a caustic the travel time difference $t_{SB} - t_{SA} = t_{AB}$ does not change to second order with the source position. At a general caustic in two dimensions, the travel time difference $t_{SB} - t_{SA}$ thus has a vanishing curvature with respect to the source location, which is the behavior discussed in the previous section. The conclusion of that section thus carry over to a general caustic in two dimensions.

In three dimensions there are two take-off angles γ_1 and γ_2, and the condition for a caustic is [*Berry and Upstill*, 1980]

$$\det \frac{\partial^2 t_{AB}}{\partial \gamma_i \partial \gamma_j} = 0 \quad \text{(caustic)} . \tag{16}$$

Since the change in each take-off angle corresponds to a change in source coordinates, expression (16) is equivalent to

$$\det \frac{\partial^2 t_{AB}}{\partial s_i \partial s_j} = 0 \quad \text{(caustic)} , \tag{17}$$

where s_1 and s_2 are changes in the source coordinates that correspond to changes in the two take-off angles. In the stationary phase analysis of the interferometric integral (1) the final result is proportional to $1/\sqrt{\det(\partial^2 t_{AB}/\partial s_i \partial s_j)}$ (expression (24.42) of *Snieder and van Wijk* [2015]). At a caustic, where expression (17) holds, a second-order stationary-phase analysis thus predicts an infinite amplitude. For a general caustic, the contribution from the stationary point comes from the contributions in the source position that vary to the third order or higher. This variation is related with the topology of the caustic and is different for a fold, a cusp, a swallowtail, and other types of caustics. The resulting amplitude and diffraction pattern at the caustic also depends on the topology of the caustic [*Berry and Upstill*, 1980; *Nye*, 1999].

On a spherically symmetric Earth the antipode is always at a caustic. To see this we use a system of spherical coordinates with the north pole at the source. When the angles θ and φ in this system of spherical coordinates are used to characterize the take-off angles of a ray, the determinant (17) at the antipode is given by

$$\begin{vmatrix} \dfrac{\partial^2 t}{\partial \theta^2} & \dfrac{\partial^2 t}{\partial \theta \partial \varphi} \\[2mm] \dfrac{\partial^2 t}{\partial \theta \partial \varphi} & \dfrac{\partial^2 t}{\partial \varphi^2} \end{vmatrix} = \begin{vmatrix} \dfrac{\partial^2 t}{\partial \theta^2} & 0 \\[2mm] 0 & 0 \end{vmatrix} = 0 . \tag{18}$$

The first identity follows from the fact that at the antipode the travel time does not depend on the azimuth of the take-off direction, so that $\partial t/\partial \varphi = \partial^2 t/\partial \varphi^2 = 0$. The second identity implies that the antipode is indeed a caustic. Physically speaking, at the antipode, rays arrive with identical travel times from all azimuths. Note that aspherical Earth structure causes triplications in the antipodal caustics, this is shown for surface waves by *Wang et al.* [1993]. At such a triplicated caustic the amplitude is still large, but it is not clear what the implications are for the interferometric reconstruction of waves at antipodal stations.

5. A Simple Example of Stationary Phase Integration

As discussed in the previous section, for interferometry at caustics, the stationary phase zones are wider than at other locations, which increases the probability that noise sources are located in the stationary phase zone.
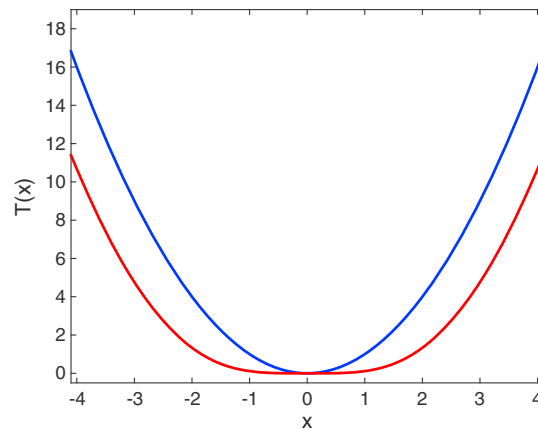
Figure 7. Times $T_2(x)$ (blue) and $T_4(x)$ (red) defined in equation (19).

But does this mean that one needs a smaller number of sources? We address this question in this section with a simplified model for the evaluation of the interferometric integral (1) by summing the contributions from a limited number of sources.

We define travel time differences that are prototypes of the travel time differences shown by the red curves in Figures 5a and 5b. In the example, we define the following travel times as a function of a dimensionless variable x (defined as distance divided by wavelength):

$$T_2(x) = x^2 \quad \text{and} \quad T_4(x) = \frac{x^4}{x^2 + 8} . \tag{19}$$

These travel times are shown in Figure 7. The travel time $T_2(x)$ is parabolic and is similar to the red curve in Figure 5a, while $T_4(x)$ varies near the stationary point $x = 0$ as x^4, as does the travel time difference shown by the red curve in Figure 5b. Note that for large values of x, both functions behave as x^2. We use these functions on the interval $-x_0 < x < x_0$ with $x_0 = 8$ and mimic the interferometric integral by defining

$$F_n(x) = \left(1 - (x/x_0)^2\right) \cos T_n(x) , \tag{20}$$

for $n = 2$ and $n = 4$. These functions are shown in Figure 8. Note that both functions are oscillatory but have a stationary phase region at $x = 0$. Away from a caustic (blue curve), the function behaves as x^2 near the stationary point, while at a caustic (red curve), the function behaves as x^4. As a result the stationary phase region is larger for the red curve than for the blue curve. Note that the oscillatory behavior of the two functions away from the stationary phase region is identical.

The true value of the integrals $\int_{-x_0}^{x_0} F_2(x)dx$ and $\int_{-x_0}^{x_0} F_4(x)dx$ is shown by the horizontal blue and red lines in Figure 9, respectively. For the case of a caustic (red line and symbols), the integral is larger than it is away from a caustic (blue line and symbols). This corresponds to the larger area of the stationary phase region of the red curve in Figure 8 than of the blue line in that figure.

In seismic interferometry, the integration in expression (1) is usually carried our implicitly by using noise that is generated by a number of randomly distributed sources. In our example we mimic this by evaluating the integrals $\int_{-x_0}^{x_0} F_n(x)dx$ by a Monte Carlo integration over N points that are randomly chosen along the interval $-x_0 < x < x_0$. The resulting estimates are shown in Figure 9 as a function of the number of sampling points N for $F_2(x)$ (blue dots) and $F_4(x)$ (red dots).
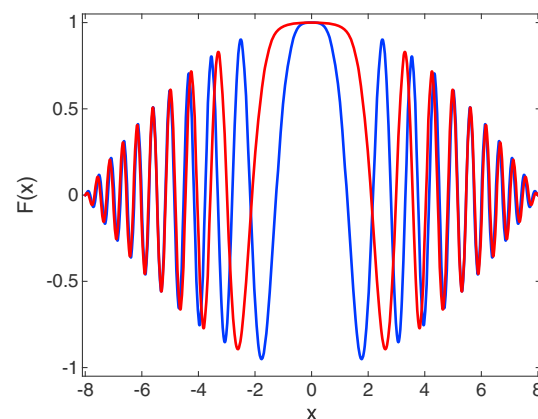
For both functions the Monte Carlo estimates approach the true values of the integrals as the number of sampling points N increases. Note that even for this simple problem one needs a fairly large number of sampling points (sources) to accurately estimate the interferometric integral. This is consistent with the findings of *Fan and Snieder* [2009] who showed that one needs several sources per wavelength in seismic interferometry. They also showed that one needs more sources when the sources have random locations instead of a regular distribution of sources. Perhaps surprisingly, they also showed that one also needs a large number of sources for strongly scattering media.
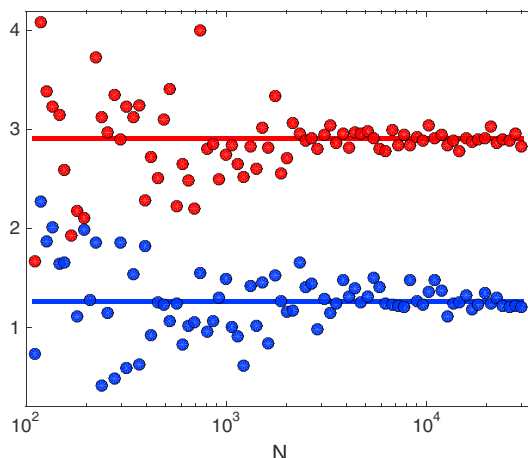

Figure 8. Functions $F_2(x)$ (blue) and $F_4(x)$ (red) defined in equation (20).

Figure 9. True values of the integrals $\int F_2(x)dx$ (blue horizontal line) and $\int F_4(x)dx$ (red horizontal line), as well as estimates from Monte Carlo sampling using N randomly chosen points.

The fluctuations of the Monte Carlo estimates in Figure 9 around the true value are comparable for the two functions. The reason is that these fluctuations are due to the random sampling of the oscillatory parts of the functions $F_2(x)$ and $F_4(x)$. The contribution of the oscillatory parts should integrate to zero, but with an inadequate sampling this does not happen. This oscillatory behavior of the functions $F_2(x)$ and $F_4(x)$ in Figure 8 is similar; hence, the fluctuations in the Monte Carlo estimates behave similarly as well. However, because of the larger value of the integral of $F_4(x)$, the relative size of the fluctuations is less for $F_4(x)$ than for $F_2(x)$.

In seismic interferometry, a finite number of noise sources lead to deviations of the extracted Green's functions from the real one. If these deviations are of the same order as the Green's function itself, the coherency of the extracted waveform is lost. This is less likely to happen at a caustic because at these locations the waves are stronger than at other locations. In terms of the integrand of the interferometric integral (1) this large amplitude corresponds to a wide stationary phase region.

6. Conclusions

The special example in section 3 and its generalization to general caustics in section 4 show that when receiver B is at a caustic for rays leaving receiver A, the travel time difference in the interferometric integral (1) has a vanishing curvature at the stationary point. This causes a slow variation of the travel time difference compared to a stationary point with a nonzero curvature (compare the red curve in Figure 5b with the red curves in Figures 5a and 5c). As a result, the stationary phase zone of the interferometric integral (1) is much wider at a caustic than at other locations.

This increased width of the stationary phase zone at a caustic has consequences for the extraction of body waves. First, for a homogeneous distribution of sources, a wider stationary phase zone contains more sources than a narrower stationary phase zone. Therefore, more sources (either real or secondary sources) contribute to the extraction of the wave field at a caustic than at other locations. As a result, the amplitude of the wave field extracted from seismic interferometry is larger as well. This large amplitude corresponds to the large amplitude of the waves at a caustic. The example of Figure 9 shows that the absolute errors in the extracted waves for a limited number of sources are about equal for a regular stationary phase integration and for the stationary phase integral at a caustic. The relative errors are, however, smaller for waves at a caustic than at other locations because of the larger number of sources in the stationary phase zone.

It has been argued earlier that reverberations *Boué et al.* [2014] and scattering [*Snieder and Fleury*, 2010] create additional stationary phase zones, which makes it more likely that sources are present in the stationary phase zones. This is similar to the widening of stationary phase regions at caustics that we show in this work. The creation of new stationary phase zones by reverberation or scattering, and the widening of stationary phase zones at caustics both make it more likely that sources are present in regions that contribute to the interferometric integral.

It has been argued earlier that the stationary phase zone for body waves is much smaller than it is for surface waves [*Forghani and Snieder*, 2010]. The ability to extract body waves from seismic interferometry depends on a number of factors that include the distribution of scatterers and noise sources, the attenuation in the Earth, the presence of reverberations, and as we show in this work, receivers near caustics. It is the interplay and possible combination of these factors that determine our ability to retrieve body waves from seismic interferometry.
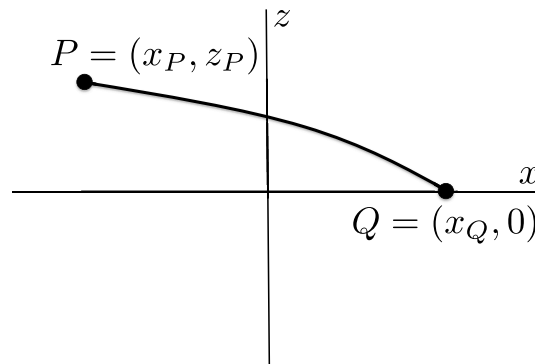
Figure A1. Definition of geometric variables used for the computation of a ray.

Appendix A: Computation of the Rays and Travel Times

The rays satisfy the equation of kinematic ray tracing

$$\frac{d}{ds}\left(\frac{1}{c}\frac{d\mathbf{r}}{ds}\right) = \nabla\left(\frac{1}{c}\right) , \tag{A1}$$

where s is the arc length along the ray. Since the example of the waveguide is illustrative only, we make a number of approximations to simplify the problem and bring out the essential physics. We consider rays that propagate nearly parallel to the axis of the waveguide. In that case we can replace the s derivatives in expression (A1) by x derivatives. We replace $1/c$ in the left hand side by $1/c_0$. Taking the z component of the result and using expression (2) in the right-hand side gives

$$\frac{d^2z}{dx^2} = -q^2z . \tag{A2}$$

The used approximations are valid when

$$\left(\frac{dz}{dx}\right) \ll 1 \quad \text{and} \quad q^2z^2 \ll 1 . \tag{A3}$$

In this problem we consider rays that propagate from a general point P to a point Q on the x axis, see Figure A1. The general solution of equation (A2) is a superposition of $\cos q(x_Q - x)$ and $\sin q(x_Q - x)$. For the rays shown in Figure A1, the solution is given by

$$z(x) = z_P \frac{\sin q(x_Q - x)}{\sin q(x_Q - x_P)} . \tag{A4}$$

When $z_P = 0$, the ray moves along the axis of the waveguide ($z(x) = 0$), except when $\sin q(x_Q - x_P) = 0$. In that case rays that start in the center of the waveguide oscillate along the x axis and converge on point Q. In that case the point Q is at a caustic; hence, the condition for being at a caustic is

$$\sin q(x_Q - x_P) = 0 \quad \text{(caustic)} . \tag{A5}$$

For the rays in Figure 1, $(x_Q, z_Q) = (-D, z)$. For the ray ending at receiver A, $(x_P, z_P) = (0, 0)$, while for the ray ending at receiver B, $(x_P, z_P) = (L, 0)$. Inserting this in the solution (A4) gives equations (3) and (4).

The travel time is given by $t = \int (1/c)ds$. Using the velocity profile from equation (2) and $ds = \sqrt{1 + (dz/dx)^2}\, dx$, one obtains

$$t = \frac{1}{c_0} \int_{x_P}^{x_Q} \left(1 - q^2z^2/2\right) \sqrt{1 + (dz/dx)^2}\, dx . \tag{A6}$$

A Taylor expansion of expression (A6) in z shows that the zeroth and second-order dependence of the travel time on z is given by

$$t^{(0)} = \frac{x_Q - x_P}{c_0} \quad \text{and} \quad t^{(2)} = \frac{1}{2c_0} \int_{x_P}^{x_Q} \left((dz/dx)^2 - q^2z^2\right) dx \tag{A7}$$

For the ray (A4) the second-order travel time variation is given by

$$t^{(2)} = \frac{qz_P^2}{2c_0 \tan q(x_Q - x_P)} . \tag{A8}$$

The conditions (A3) used for the validity of the used ray estimates imply with equation (A6) that the travel time must be close to the travel time $(x_Q - x_P)/c_0$ along the x axis. This means that the reduced travel time, defined in expression (13) must satisfy $|t_{reduced}| \ll t(z = 0)$. A comparison of Figures 4 and 5 shows that in the examples used $|t_{reduced}|/t(z = 0) \sim 1\% \ll 1$, so that the requirements (A3) for the used ray approximations are indeed satisfied.

References

Aki, K., and P. Richards (2002), *Quantitative Seismology*, 700 pp., 2nd ed., Univ. Science Books, Sausalito, Calif.

Aldridge, D. (1994), Linearization of the eikonal equation, *Geophysics*, 59, 1631–1632.

Bakulin, A., and R. Calvert (2006), The virtual source method: Theory and case study, *Geophysics*, 71, SI139–SI150.

Bender, C., and S. Orszag (1978), *Advanced Mathematical Methods for Scientists and Engineers*, McGraw-Hill, New York.

Berry, M., and C. Upstill (1980), Catastrophe optics: Morphologies of caustics and their diffraction patterns, in *Prog. in Optics*, vol. 18, edited by E. Wolf, pp. 257–346, North Holland, Amsterdam.

Bharadwaj, P., T. Nissen-Meyer, G. Schuster, and P. Mai (2014), Enhanced core-diffracted arrivals by supervirtual interferometry, *Geophys. J. Int.*, 196, 1177–1188.

Bostock, M., and S. Rondenay (1999), Migration of scattered teleseismic body waves, *Geophys. J. Int.*, 137, 732–746.

Bostock, M., R. Hyndman, S. Rondenay, and S. Peacock (2002), An inverted continental Moho and serpentinization of the forearc mantle, *Nature*, 417, 536–538.

Boué, P., P. Poli, M. Campillo, H. Pedersen, X. Briand, and P. Roux (2013), Teleseismic correlations of ambient seismic noise for deep global imaging of the Earth, *Geophys. J. Int.*, 194, 844–848.

Boué, P., P. Poli, M. Campillo, and P. Roux (2014), Reverberations, coda waves and ambient noise: Correlations at the global scale and retrieval of deep phases, *Earth Planet. Sci. Lett.*, 391, 137–145.

Campillo, M., and A. Paul (2003), Long-range correlations in the diffuse seismic coda, *Science*, 299, 547–549.

Campillo, M., H. Sato, N. Shapiro, and R. van der Hilst (2011), New developments on imaging and monitoring with seismic noise, *C. R. Geosci.*, 343, 487–495.

Chapman, C. (2004), *Fundamentals of Seismic Wave Propagation*, Cambridge Univ. Press, Cambridge, U. K.

Curtis, A., P. Gerstoft, H. Sato, R. Snieder, and K. Wapenaar (2006), Seismic interferometry—Turning noise into signal, *The Leading Edge*, 25, 1082–1092.

Dietrich, G., K. Kalle, W. Krauss, and G. Siedler (1980), *General Oceanography*, 2nd ed., John Wiley, New York.

Draganov, D., X. Campman, J. Thorbecke, A. Verdel, and K. Wapenaar (2009), Reflection images from ambient seismic noise, *Geophysics*, 74, A63–A67.

Fan, Y., and R. Snieder (2009), Required source distribution for interferometry of waves and diffusive fields, *Geophys. J. Int.*, 179, 1232–1244.

Forghani, F., and R. Snieder (2010), Underestimation of body waves and feasibility of surface-wave reconstruction by seismic interferometry, *The Leading Edge*, 29, 790–794.

Gerstoft, P., P. Shearer, N. Harmon, and J. Zhang (2008), Global P, PP, and PKP wave microseisms observed from distant storms, *Geophys. Res. Lett.*, 35, L23306, doi:10.1029/2008GL036111.

Kumar, M., and M. Bostock (2006), Transmission to reflection transformation of teleseismic wavefields, *J. Geophys. Res.*, 111, B08306, doi:10.1029/2005JB004104.

Larose, E. (2006), Mesoscopics of ultrasound and seismic waves: Applications to passive imaging, *Ann. Phys. Fr.*, 31, 1–126.

Larose, E., L. Margerin, A. Derode, B. van Tiggelen, M. Campillo, N. Shapiro, A. Paul, L. Stehly, and M. Tanter (2006), Correlation of random wavefields: An interdisciplinary review, *Geophysics*, 71, SI11–SI21.

Lin, F., and V. C. Tsai (2013), Seismic interferometry with antipodal station pairs, *Geophys. Res. Lett.*, 40, 4609–4613, doi:10.1002/grl.50907.

Lin, F., V. Tsai, B. Schmandt, Z. Duputel, and Z. Zhan (2013), Extracting core phases with array interferometry, *Geophys. Res. Lett.*, 40, 1049–1053, doi:10.1002/grl.50237.

Mikesell, D., and K. van Wijk (2011), Seismic refraction interferometry with a semblance analysis on the crosscorrelation gathering, *Geophysics*, 76, SA77–SA82.

Nakata, N., R. Snieder, T. Tsuji, K. Larner, and T. Matsuoka (2011), Shear wave imaging from traffic noise using seismic interferometry by cross-coherence, *Geophysics*, 76, SA97–SA106.

Nishida, K. (2013), Global propagation of body waves revealed by cross-correlation analysis of seismic hum, *Geophys. Res. Lett.*, 40, 1691–1696, doi:10.1002/grl.50269.

Nye, J. (1999), *Natural Focusing and Fine Structure of Light*, Institute of Physics, Bristol, U. K.

Poli, P., H. Pedersen, M. Campillo, and P. W. Group (2012a), Emergence of body waves from cross-correlation of short period seismic noise, *Geophys. J. Int.*, 188, 549–558.

Poli, P., M. Campillo, H. Pedersen, and L. W. Group (2012b), Mantle discontinuities from ambient seismic noise, *Science*, 338, 1063–1065.

Ritzwoller, M., F.-C. Lin, and W. Shen (2011), Ambient noise tomography with a large seismic arrays, *C. R. Geosci.*, 343, 558–570.

Roux, P., W. Kuperman, and N. Group (2004), Extracting coherent wave fronts from acoustic ambient noise in the ocean, *J. Acoust. Soc. Am.*, 116, 1995–2003.

Ruigrok, E., X. Campman, and K. Wapenaar (2011), Extraction of P-wave reflections from microseisms, *C. R. Geosci.*, 343, 512–525.

Schulte-Pelkum, V., P. Earle, and F. Vernon (2004), Strong directivity of ocean-generated seismic noise, *Geochem. Geophys. Geosyst.*, 5, Q03004, doi:10.1029/2003GC000520.

Snieder, R. (2004), Extracting the Green's function from the correlation of coda waves: A derivation based on stationary phase, *Phys. Rev. E.*, 69, 046610.

Snieder, R., and C. Fleury (2010), Cancellation of spurious arrivals in Green's function retrieval of multiple scattered waves, *J. Acoust. Soc. Am.*, 128, 1598–1605.

Snieder, R., and E. Larose (2013), Extracting Earth's elastic wave response from noise measurements, *Annu. Rev. Earth Planet. Sci.*, 41, 183–206.

Snieder, R., and K. van Wijk (2015), *A Guided Tour of Mathematical Methods for the Physical Sciences*, 560 pp., 3rd ed., Cambridge Univ. Press, Cambridge, U. K.

Snieder, R., K. Wapenaar, and K. Larner (2006), Spurious multiples in seismic interferometry of primaries, *Geophysics*, 71, SI111–SI124.

Snieder, R., K. van Wijk, M. Haney, and R. Calvert (2008), The cancellation of spurious arrivals in Green's function extraction and the generalized optical theorem, *Phys. Rev. E.*, 78, 036606.

Stehly, L., M. Campillo, and N. Shapiro (2006), A study of seismic noise from long-range correlation properties, *J. Geophys. Res.*, 111, B10306, doi:10.1029/2005JB004237.

Traer, J., and P. Gerstoft (2014), A unified theory of microseisms and hum, *J. Geophys. Res. Solid Earth*, 119, 3317–3339, doi:10.1002/2013JB010504.

Wang, Z., F. Dahlen, and J. Tromp (1993), Surface wave caustics, *Geophys. J. Int.*, 114, 311–324.

Wapenaar, K., and J. Fokkema (2006), Green's function representations for seismic interferometry, *Geophysics*, 71(4), SI33–SI46.

Zhan, Z., S. Ni, D. Helmberger, and R. Clayton (2010), Retrieval of Moho-reflected shear wave arrivals from ambient seismic noise, *Geophys. J. Int.*, 182, 408–420.

Zhang, J., P. Gerstoft, and P. Shearer (2009), High-frequency P-wave seismic noise driven by ocean winds, *Geophys. Res. Lett.*, 36, L09302, doi:10.1029/2009GL037761.